Crystal structures and elastic properties of superhard IrN_2 and IrN_3 from first principles

Zhi-jian Wu,[1,*] Er-jun Zhao,[1,2] Hong-ping Xiang,[1,2] Xian-feng Hao,[1,2] Xiao-juan Liu,[1] and Jian Meng[1]
[1]*Key Laboratory of Rare Earth Chemistry and Physics, Changchun Institute of Applied Chemistry, Chinese Academy of Sciences, Changchun 130022, People's Republic of China*
[2]*Graduate School, Chinese Academy of Sciences, Beijing 100049, People's Republic of China*
(Received 7 November 2006; revised manuscript received 25 March 2007; published 14 August 2007; corrected 27 August 2007)

First principles calculations were performed to investigate the structural, elastic, and electronic properties of IrN_2 for various space groups: cubic *Fm*-3*m* and *Pa*-3, hexagonal $P3_221$, tetragonal $P4_2/mnm$, orthorhombic *Pmmn*, *Pnnm*, and *Pnn*2, and monoclinic $P2_1/c$. Our calculation indicates that the $P2_1/c$ phase with arsenopyrite-type structure is energetically more stable than the other phases. It is semiconducting (the remaining phases are metallic) and contains diatomic N-N with the bond distance of 1.414 Å. These characters are consistent with the experimental facts that IrN_2 is in lower symmetry and nonmetallic. Our conclusion is also in agreement with the recent theoretical studies that the most stable phase of IrN_2 is monoclinic $P2_1/c$. The calculated bulk modulus of 373 GPa is also the highest among the considered space groups. It matches the recent theoretical values of 357 GPa within 4.3% and of 402 GPa within 7.8%, but smaller than the experimental value of 428 GPa by 14.7%. Chemical bonding and potential displacive phase transitions are discussed for IrN_2. For IrN_3, cubic skutterudite structure (*Im*-3) was assumed. Our calculation indicated that it is also promising to be superhard due to the large bulk modulus of 358 GPa and shear modulus of 246 GPa. The diatomic N-N bond distance is even shorter (1.272 Å).

DOI: 10.1103/PhysRevB.76.054115 PACS number(s): 61.50.Ah, 71.15.Mb, 71.20.Be

INTRODUCTION

Due to the importance in fundamental science and technological applications, superhard materials have been studied both theoretically and experimentally.[1–27] In the recent theoretical studies, hypothetical hard structures of carbon with cubic symmetry, i.e., body centered C_6 with 12 atoms per unit cell and simple cubic C_{20} with 20 atoms per unit cell, were studied by density functional theory (DFT).[3] It turns out to be that both structures have similar bulk moduli of about 350 GPa at ambient conditions.[3] Conducting superhard tetragonal BC_3 phase, which originates from cubic diamond structure, was predicted by first principles.[4] In addition, Vickers hardness was calculated for five predicted C_3N_4 polymorphs.[5] It was found that cubic C_3N_4 is the hardest, with the hardness of 92 GPa.[5] Besides the studies on compounds containing carbon atom, the compounds containing both nitrogen and transition metal atoms have also been the focus of recent studies, in particular, for binary transition metal nitrides.[6–27] The recent review paper of Horvath-Bordon *et al.* is an excellent guide for the nitride materials.[6] Individual studies on the binary transition metal nitride include the experimental synthesis of novel Hf_3N_4 with the thorium phosphide (Th_3P_4) structure in the diamond-anvil cell at 18 GPa and 2800 K,[7] and high temperature and high pressure synthesis of novel platinum nitride at above 45–50 GPa and temperature exceeding 2000 K.[8] Meanwhile, first principles studies were conducted on Hf_3N_4,[9–11] Zr_3N_4,[9–11] Ti_3N_4,[10,11] Ta_3N_5,[12] and WN_2.[12] For Ta_3N_5 and WN_2, novel phases were predicted.[12] For platinum nitride, PtN (stoichiometry 1:1) at various structures,[13,14] PtN_2 (stoichiometry 1:2),[14] and nonstoichiometric PtN_x, with x changing from 0.95 to 1.25,[14] were examined theoretically in order to find the most stable phase. It was found that pyrite PtN_2 is the most stable,[14] in agreement with the recent experimental observation.[15]

Most recently, three new transition metal nitrides, i.e., osmium nitride,[16] iridium nitride,[15,16] and platinum nitride,[15] were synthesized at high pressures and high temperatures. These studies suggested that the three compounds have a metal: nitrogen stoichiometry of 1:2,[15,16] but the detailed crystal structure remains elusive, especially for OsN_2 and IrN_2. For PtN_2, early theoretical study suggested that fluorite structure is the most stable phase.[17,18] Later, it was confirmed that pyrite structure is energetically more favorable than fluorite structure.[14,15,19–21] For OsN_2, theoretical study was conducted on both fluorite and pyrite structures.[22] This is different from the experimental observation that OsN_2 is orthorhombic.[16] Therefore, further theoretical studies were made, focusing on the orthorhombic phase. It was found that marcasite structure is the most sable phase for OsN_2.[23–27]

For IrN_2, however, the determination of crystal structure is more difficult. This is partly due to the fact that for IrN_2, the intensity ratio of x-ray diffraction peaks between nitride and pure metal is 1:100, much weaker than 1:3 for OsN_2 and 1:10 for PtN_2.[16] The measured bulk modulus of IrN_2 is high[16] (428 GPa) and matches that of diamond (440 GPa) within 5%. Although the crystal structure was not determined, it was suggested that the searches on IrN_2 are restricted to the structures with even number of formula units to fulfill the requirement of nonmetallicity and with threefold symmetry.[16] In addition, the structure should also contain the single-bonded diatomic N-N units.[16] Therefore, since the crystal structure of IrN_2 is questionable, in the present study, based on the experimental study (but not restricted by the experimental study), we have studied the various possible structures of IrN_2 by first principles calculations. The structures we considered are based on the chemically related compounds and summarized in the following. Cubic phases *Fm*-3*m* (fluorite, prototype CaF_2, No. 225) and *Pa*-3 (pyrite, prototype FeS_2, No. 205) were considered because, on the

studies of PtN_2, both fluorite[17,18] and pyrite structures[14,15,19–21] were adopted, with the latter energetically more stable than the former. Hexagonal phase $P3_221$ (No. 154) was chosen because it was suggested in the recent experimental study.[16] Since IrO_2 with tetragonal $P4_2/mnm$ (No. 136) phase was synthesized experimentally,[28] it was adopted as well. In addition, three space groups of the orthorhombic system were considered, which are *Pmmn*, No. 59 from OsB_2,[29] and *Pnnm* No. 58 (Ref. 30) and *Pnn*2 No. 34 (Ref. 31) from marcasite FeS_2. Finally, since monoclinic arsenopyrite structure $P2_1/c$ ($CoSb_2$ or FeAsS type) was observed for IrP_2,[32] $IrAs_2$,[32] $IrSb_2$,[33] $IrBi_2$,[34] CoP_2,[35] and RhP_2,[32] it was also chosen as one of the potential candidates. From previous study,[32] it is known that FeS_2-pyrite, FeS_2-marcasite, and $CoSb_2$ or FeAsS-arsenopyrite structures are dominant for binary compounds, with a frequency of occurence in the given order. From the recent studies on binary transition metal nitride, it is interesting to note that for PtN_2, pyrite structure is the most stable,[14,15,19–21] while for OsN_2, marcasite structure is the most stable.[23–27] From our study and the works of Yu *et al.*[27] and Wang *et al.*,[36] $CoSb_2$ or FeAsS-arsenopyrite structure is the most stable for IrN_2.

Since the structures with threefold symmetry were suggested by the experimental study,[16] besides $P3_221$ mentioned earlier, we have also chosen three more hexagonal systems as observed in WB_2 [$P6_3/mmc$, No 196 (Ref. 37); $P6/mmm$, No. 191 (Ref. 38)], ReB_2 ($P6_3/mmc$, No. 196),[39] and trigonal system as observed in WN_2 (R-3m, No. 166).[40] It turns out that when IrN_2 was assumed to adopt these structures ($P6_3/mmc$, $P6/mmm$, and R-3m), significant structural distortion was observed during the geometry optimization and the assumed structures are mechanically unstable.

On the other hand, since it was suggested by the experiment that for IrN_x, x can be 2 ± 0.5,[15] therefore, besides IrN_2, iridium nitride with both the other stoichiometries and nonstoichiometry should be examined. We, thus, performed calculations on both IrN and IrN_3. For IrN, we choose four structures, i.e., zinc blende (ZnS), rocksalt (NaCl), tungsten carbide (WC), and cesium chloride (CsCl). It turns out that only in zinc blende structure is IrN mechanically stable. Although the calculated bulk modulus is large [283 GPa at the generalized gradient approximation (GGA) level], the calculated shear modulus is quite small (around 10 GPa). Therefore, we did not present these results in this paper.

For IrN_3, it was examined by assuming the skutterudite structure ($CoAs_3$ type, cubic system, space group Im-3, No. 204). Similar to IrN_2, the structure was adopted because IrP_3,[41] $IrAs_3$,[42] $IrSb_3$,[42] CoP_3,[41] and RhP_3 (Ref. 41) were synthesized with cubic skutterudite $CoAs_3$ type structure. Our calculated bulk modulus is 358 GPa and shear modulus is 246 GPa. This shows that IrN_3 could be a potential candidate to be superhard. The detailed results are presented in this paper. In addition, the iridium nitride with nonstoichiometry or vacancy and/or defects should also be examined because there might also be a good chance to find a superhard candidate.[43] Our work on this side is under way.

COMPUTATIONAL DETAILS

In the present work, DFT is used as implemented in the CASTEP code.[44] The Vanderbilt ultrasoft pseudopotential[45] was used with the same cutoff energy of 310 eV for the considered structures in IrN_2. The k points of $6\times6\times6$ for cubic Fm-3m and Pa-3, $8\times8\times4$ for hexagonal $P3_221$, $5\times5\times8$ for tetragonal $P4_2/mnm$, $4\times10\times8$ for orthorhombic $Pmmn$, $6\times5\times9$ for orthorhombic $Pnnm$ and $Pnn2$, and $5\times5\times5$ for monoclinic $P2_1/c$ are generated using the Monkhorst-Pack scheme.[46] For IrN_3, we choose the cutoff energy of 400 eV and k points of $4\times4\times4$. The conventional cell which contains 8 f.u. (i.e., eight IrN_3) is used for IrN_3 during the geometry optimization. The exchange and correlation functional are treated by both the local density approximation[47] (LDA) and the GGA.[48] Since it is known that LDA usually underestimates the lattice constants and overestimates the elastic constants, while GGA overestimates the lattice constants and underestimates the elastic constants, the arithmetic average of LDA and GGA values were used as the theoretical value. The tolerances for geometry optimization were set as the difference in total energy being within 5×10^{-6} eV/atom, the maximum ionic Hellmann-Feynman force within 0.01 eV/Å, the maximum ionic displacement within 5×10^{-4}Å, and the maximum stress within 0.02 GPa. Formation enthalpies were calculated from $\Delta E = E(IrN_2)$-E(solid Ir)-E(solid molecular N_2) for IrN_2 and $\Delta E = E(IrN_3)$-E(solid Ir)-(3/2)E(solid molecular N_2) for IrN_3. The solid molecular N_2 is from its α phase.[49] The calculated bulk and shear moduli are from the Voigt-Reuss-Hill approximations.[50–52] The pressure is applied by the equivalent hydrostatic pressure.

In the following section, we will introduce the formulas of elastic moduli and mechanical stability criteria for the considered crystal systems. The formulas of elastic moduli for cubic phase are from Ref. 1, tetragonal and hexagonal phases from Ref. 53, orthorhombic phase from Ref. 54, and monoclinic phase from Ref. 55. Mechanical stability criteria are from Ref. 56. In the following formulas, subscript V denotes the Voigt bound, R denotes the Reuss bound, and H denotes the Hill average. It is known that the Voigt bound is obtained by the average polycrystalline moduli based on an assumption of uniform strain throughout a polycrystal and is the upper limit of the actual effective moduli,[50] while the Reuss bound is obtained by assuming a uniform stress and is the lower limit of the actual effective moduli.[51] The arithmetic average of Voigt and Reuss bounds is termed as the Voigt-Reuss-Hill approximations.[52] B indicates bulk modulus, G shear modulus, E Young's modulus, and ν Possion's ratio. It should be mentioned that the Reuss bound can also be represented by the elastic compliance coefficients s_{ij}, but in this paper, we use the elastic stiffness constants C_{ij} instead to represent the Reuss bound.

Cubic phase (C_{11}, C_{44}, and C_{12})

$$B_V = B_R = (C_{11} + 2C_{12})/3,$$

$$G_V = (C_{11} - C_{12} + 3C_{44})/5,$$

$$G_R = 5(C_{11} - C_{12})C_{44}/[4C_{44} + 3(C_{11} - C_{12})].$$

The mechanical stability criteria are given by

$$C_{11} > 0, \quad C_{44} > 0, \quad C_{11} > |C_{12}|, \quad (C_{11} + 2C_{12}) > 0.$$

Hexagonal phase (C_{11}, C_{33}, C_{44}, C_{12}, and C_{13})

$$B_V = (1/9)[2(C_{11} + C_{12}) + 4C_{13} + C_{33}],$$

$$G_V = (1/30)(M + 12C_{44} + 12C_{66}),$$

$$B_R = C^2/M,$$

$$G_R = (5/2)[C^2 C_{44} C_{66}]/[3B_V C_{44} C_{66} + C^2(C_{44} + C_{66})],$$

$$M = C_{11} + C_{12} + 2C_{33} - 4C_{13},$$

$$C^2 = (C_{11} + C_{12})C_{33} - 2C_{13}^2.$$

The mechanical stability criteria are given by

$$C_{44} > 0, \quad C_{11} > |C_{12}|, \quad (C_{11} + 2C_{12})C_{33} > 2C_{13}^2.$$

Tetragonal phase (C_{11}, C_{33}, C_{44}, C_{66}, C_{12}, and C_{13})

$$B_V = (1/9)[2(C_{11} + C_{12}) + C_{33} + 4C_{13}],$$

$$G_V = (1/30)(M + 3C_{11} - 3C_{12} + 12C_{44} + 6C_{66}),$$

$$B_R = C^2/M,$$

$$G_R = 15\{(18B_V/C^2) + [6/(C_{11} - C_{12})] + (6/C_{44}) + (3/C_{66})\}^{-1},$$

$$M = C_{11} + C_{12} + 2C_{33} - 4C_{13},$$

$$C^2 = (C_{11} + C_{12})C_{33} - 2C_{13}^2.$$

The mechanical stability criteria are given by

$$C_{11} > 0, \quad C_{33} > 0, \quad C_{44} > 0, \quad C_{66} > 0,$$
$$(C_{11} - C_{12}) > 0, \quad (C_{11} + C_{33} - 2C_{13}) > 0,$$
$$[2(C_{11} + C_{12}) + C_{33} + 4C_{13}] > 0.$$

Orthorhombic phase (C_{11}, C_{22}, C_{33}, C_{44}, C_{55}, C_{66}, C_{12}, C_{13}, and C_{23})

$$B_V = (1/9)[C_{11} + C_{22} + C_{33} + 2(C_{12} + C_{13} + C_{23})],$$

$$G_V = (1/15)[C_{11} + C_{22} + C_{33} + 3(C_{44} + C_{55} + C_{66}) - (C_{12} + C_{13} + C_{23})],$$

$$B_R = \Delta[C_{11}(C_{22} + C_{33} - 2C_{23}) + C_{22}(C_{33} - 2C_{13}) - 2C_{33}C_{12} + C_{12}(2C_{23} - C_{12}) + C_{13}(2C_{12} - C_{13}) + C_{23}(2C_{13} - C_{23})]^{-1},$$

$$G_R = 15\{4[C_{11}(C_{22} + C_{33} + C_{23}) + C_{22}(C_{33} + C_{13}) + C_{33}C_{12} - C_{12}(C_{23} + C_{12}) - C_{13}(C_{12} + C_{13}) - C_{23}(C_{13} + C_{23})]/\Delta + 3[(1/C_{44}) + (1/C_{55}) + (1/C_{66})]\}^{-1},$$

$$\Delta = C_{13}(C_{12}C_{23} - C_{13}C_{22}) + C_{23}(C_{12}C_{13} - C_{23}C_{11}) + C_{33}(C_{11}C_{22} - C_{12}^2).$$

The criteria for mechanical stability are given by

$$C_{11} > 0, \quad C_{22} > 0, \quad C_{33} > 0, \quad C_{44} > 0, \quad C_{55} > 0,$$
$$C_{66} > 0, \quad [C_{11} + C_{22} + C_{33} + 2(C_{12} + C_{13} + C_{23})] > 0,$$
$$(C_{11} + C_{22} - 2C_{12}) > 0, \quad (C_{11} + C_{33} - 2C_{13}) > 0,$$
$$(C_{22} + C_{33} - 2C_{23}) > 0.$$

Monoclinic phase (C_{11}, C_{22}, C_{33}, C_{44}, C_{55}, C_{66}, C_{12}, C_{13}, C_{23}, C_{15}, C_{25}, C_{35}, and C_{46})

$$B_V = (1/9)[C_{11} + C_{22} + C_{33} + 2(C_{12} + C_{13} + C_{23})],$$

$$G_V = (1/15)[C_{11} + C_{22} + C_{33} + 3(C_{44} + C_{55} + C_{66}) - (C_{12} + C_{13} + C_{23})],$$

$$B_R = \Omega[a(C_{11} + C_{22} - 2C_{12}) + b(2C_{12} - 2C_{11} - C_{23}) + c(C_{15} - 2C_{25}) + d(2C_{12} + 2C_{23} - C_{13} - 2C_{22}) + 2e(C_{25} - C_{15}) + f]^{-1},$$

$$G_R = 15\{4[a(C_{11} + C_{22} + C_{12}) + b(C_{11} - C_{12} - C_{23}) + c(C_{15} + C_{25}) + d(C_{22} - C_{12} - C_{23} - C_{13}) + e(C_{15} - C_{25}) + f]/\Omega + 3[g/\Omega + (C_{44} + C_{66})/(C_{44}C_{66} - C_{46}^2)]\}^{-1},$$

$$a = C_{33}C_{55} - C_{35}^2,$$

$$b = C_{23}C_{55} - C_{25}C_{35},$$

$$c = C_{13}C_{35} - C_{15}C_{33},$$

$$d = C_{13}C_{55} - C_{15}C_{35},$$

$$e = C_{13}C_{25} - C_{15}C_{23},$$

$$f = C_{11}(C_{22}C_{55} - C_{25}^2) - C_{12}(C_{12}C_{55} - C_{15}C_{25}) + C_{15}(C_{12}C_{25} - C_{15}C_{22}) + C_{25}(C_{23}C_{35} - C_{25}C_{33}),$$

$$g = C_{11}C_{22}C_{33} - C_{11}C_{23}^2 - C_{22}C_{13}^2 - C_{33}C_{12}^2 + 2C_{12}C_{13}C_{23},$$

$$\Omega = 2[C_{15}C_{25}(C_{33}C_{12} - C_{13}C_{23}) + C_{15}C_{35}(C_{22}C_{13} - C_{12}C_{23}) + C_{25}C_{35}(C_{11}C_{23} - C_{12}C_{13})] - [C_{15}^2(C_{22}C_{33} - C_{23}^2) + C_{25}^2(C_{11}C_{33} - C_{13}^2) + C_{35}^2(C_{11}C_{22} - C_{12}^2)] + gC_{55}.$$

The criteria for mechanical stability are given by

$$C_{11} > 0, \quad C_{22} > 0, \quad C_{33} > 0, \quad C_{44} > 0, \quad C_{55} > 0,$$
$$C_{66} > 0, \quad [C_{11} + C_{22} + C_{33} + 2(C_{12} + C_{13} + C_{23})] > 0,$$
$$(C_{33}C_{55} - C_{35}^2) > 0, \quad (C_{44}C_{66} - C_{46}^2) > 0,$$
$$(C_{22} + C_{33} - 2C_{23}) > 0,$$

TABLE I. Formation enthalpy per formula unit ΔE (eV), lattice constants a, b, and c (Å), β (deg) and γ (deg), cell volume per formula unit V (Å^3), and the shortest N-N and Ir-N bond distances (Å) at the GGA and LDA levels for IrN_2 from various space groups: cubic (*Fm*-3*m*, No. 225; *Pa*-3, No. 205), hexagonal ($P3_221$, No. 154), tetragonal ($P4_2/mnm$, No. 136), orthorhombic (*Pmmn*, No. 59; *Pnnm*, No. 58; *Pnn*2, No. 34), and monoclinic ($P2_1/c$, No. 14) phases. "Ave." is the average of GGA and LDA values.

		ΔE	a	b	c	β	γ	V	N-N	Ir-N
Fm-3*m*	GGA	2.64	4.911					29.6	2.455	2.126
	LDA	1.47	4.875					29.0	2.437	2.111
	Ave.		4.893					29.3	2.446	2.118
	Theor.[a]		4.842							
Pa-3	GGA	0.71	4.856					28.6	1.378	2.106
	LDA	–0.45	4.815					27.9	1.383	2.086
	Ave.		4.835					28.2	1.380	2.096
$P3_221$	GGA	1.46	3.676		7.593		120.0	29.6	1.342	2.060
	LDA	0.32	3.650		7.461		120.0	28.7	1.346	2.050
	Ave.		3.663		7.527			29.1	1.344	2.055
$P4_2/mnm$	GGA	2.11	4.623		3.138			33.5	2.558	1.990
	LDA	1.16	4.584		3.124			32.8	2.532	1.975
	Ave.		4.603		3.131			33.1	2.545	1.982
Pmmn	GGA	1.85	7.175	2.475	3.225			28.6	1.559	2.083
	LDA	0.65	7.093	2.455	3.214			28.0	1.544	2.069
	Ave.		7.134	2.465	3.219			28.3	1.551	2.076
Pnnm	GGA	0.42	4.103	4.925	2.773			28.0	1.375	2.081
	LDA	–0.78	4.082	4.890	2.744			27.4	1.378	2.062
	Ave.		4.092	4.908	2.759			27.7	1.376	2.071
*Pnn*2	GGA	0.42	4.102	4.925	2.773			28.0	1.375	2.081
	LDA	–0.78	4.082	4.890	2.744			27.4	1.378	2.062
	Ave.		4.092	4.908	2.759			27.7	1.376	2.071
$P2_1/c$	GGA	0.26	4.876	4.926	4.917	107.8		28.1	1.414	2.054
	LDA	–0.94	4.846	4.889	4.886	107.9		27.5	1.415	2.036
	Ave.		4.861	4.907	4.901	107.8		27.8	1.414	2.045
	LDA[b]		4.809	4.858	4.848	108.25		26.9		
	GGA[c]		4.8836	4.9389	4.9235	107.93		28.2		
	LDA[c]		4.8066	4.8568	4.8457	108.29		26.8		

[a]The average value of LDA and GGA values (Ref. 18).
[b]Reference 27.
[c]Reference 36.

$$[C_{22}(C_{33}C_{55}-C_{35}^2)+2C_{23}C_{25}C_{35}-C_{23}^2C_{55}-C_{25}^2C_{33}]>0,$$

$$\{2[C_{15}C_{25}(C_{33}C_{12}-C_{13}C_{23})+C_{15}C_{35}(C_{22}C_{13}-C_{12}C_{23})+C_{25}C_{35}(C_{11}C_{23}-C_{12}C_{13})]-[C_{15}^2(C_{22}C_{33}-C_{23}^2)+C_{25}^2(C_{11}C_{33}-C_{13}^2)+C_{35}^2(C_{11}C_{22}-C_{12}^2)]+C_{55}g\}>0.$$

In terms of the Voigt-Reuss-Hill approximations,[52] $M_H=(1/2)(M_R+M_V)$, $M=B$, G. Young's modulus E and Possion's ratio ν are obtained by the following formulas:

$$E=9BG/(3B+G), \quad \nu=(3B-2G)/[2(3B+G)].$$

RESULTS AND DISCUSSION

IrN_2

The calculated lattice constants and elastic stiffness constants were listed in Tables I and II, respectively. From both tables, it is seen that for the $P3_221$ phase, our calculated cell volume per formula unit is 29.4 Å^3 and bulk modulus is 271 GPa, in excellent agreement with the recent theoretical values of 29.4 Å^3 and 260 GPa,[16] and 29.04 Å^3 and 264 GPa (the average values of LDA and GGA values).[36] However, we also noticed that the optimized lattice constants (a=3.663 Å, c=7.527 Å) distorted significantly compared with the experimental values (a=3.966 Å, c=6.958 Å),[16] as

TABLE II. Elastic stiffness constants C_{ij}, bulk modulus B (GPa), shear modulus G (GPa), Young's modulus E (GPa), and Possion's ratio ν at the GGA and LDA levels for IrN_2 from various space groups: cubic (Fm-3m, No. 225; Pa-3, No. 205), hexagonal ($P3_221$, No. 154), tetragonal ($P4_2/mnm$, No. 136), orthorhombic ($Pmmn$, No. 59; $Pnnm$, No. 58; $Pnn2$, No. 34), and monoclinic ($P2_1/c$, No. 14) phases. "Ave." is the average of GGA and LDA values.

		C_{11}	C_{22}	C_{33}	C_{44}	C_{55}	C_{66}	C_{12}	C_{13}	C_{15}	C_{23}	C_{25}	C_{35}	C_{46}	B	G	E	ν
Fm-3m	GGA	375			117			312							334	69	195	0.40
	LDA	410			99			350							370	61	175	0.42
	Ave.	392			108			331							352	65	185	0.41
	Theor.[a]	428			120			306							347	92		
	GGA[b]														304			
	LDA[b]														357			
Pa-3	GGA	735			85			94							308	150	387	0.29
	LDA	839			89			131							367	161	419	0.31
	Ave.	787			87			112							337	155	403	0.30
	GGA[b]														303			
	LDA[b]														358			
$P3_221$	GGA	470		318	93			188	177						250	111	289	0.31
	LDA	550		373	105			221	205						292	128	334	0.31
	Ave.	510		345	99			204	191						271	119	311	0.31
	GGA[c]														260			
	GGA[b]														238			
	LDA[b]														290			
$P4_2/mnm$	GGA	322		553	103		273	301	217						291	83	228	0.37
	LDA	359		586	109		293	331	244						322	92	253	0.37
	Ave.	340		569	106		283	316	230						306	88	240	0.37
$Pmmn$	GGA	632	862	624	142	356	91	16	350		56				328	198	494	0.25
	LDA	657	980	692	145	391	104	24	392		64				364	214	537	0.25
	Ave.	644	921	658	143	373	97	20	371		60				346	206	515	0.25
$Pnnm$	GGA	739	883	554	124	297	190	156	277		82				345	217	538	0.24
	LDA	800	978	618	127	323	189	193	317		99				390	228	572	0.26
	Ave.	770	931	586	125	310	189	174	297		90				367	222	555	0.25
$Pnn2$	GGA	722	880	551	125	297	190	147	271		80				340	217	536	0.24
	LDA	825	987	612	126	326	195	202	333		104				396	229	575	0.26
	Ave.	773	933	581	125	311	192	174	302		92				368	223	555	0.25
$P2_1/c$	GGA	755	858	806	179	197	150	108	167	−68	129	−27	19	−27	354	224	554	0.24
	LDA	814	940	869	182	199	155	130	194	−76	151	−28	24	−32	392	231	580	0.25
	Ave.	784	899	837	180	198	152	119	180	−72	140	−27	21	−29	373	228	567	0.24
	Expt.[c]														428			
	LDA[d]														402			
	LDA[b]	797	929	852	183	192	154	130	194	−71	153	−27	19	−35	388			
	GGA[b]														327			

[a]The average value of LDA and GGA values (Ref. 18).
[b]Reference 36.
[c]Reference 16.
[d]Reference 27.

also encountered in the recent theoretical study.[16] For fluorite (Fm-3m) phase, the previous theoretical study gave a bulk modulus of 347 GPa (Ref. 18) and the recent study gave 330 GPa (the average value of LDA and GGA values),[36] in excellent agreement with our calculated value of 352 GPa (Table II). Our calculated elastic stiffness constants C_{11}, C_{44},

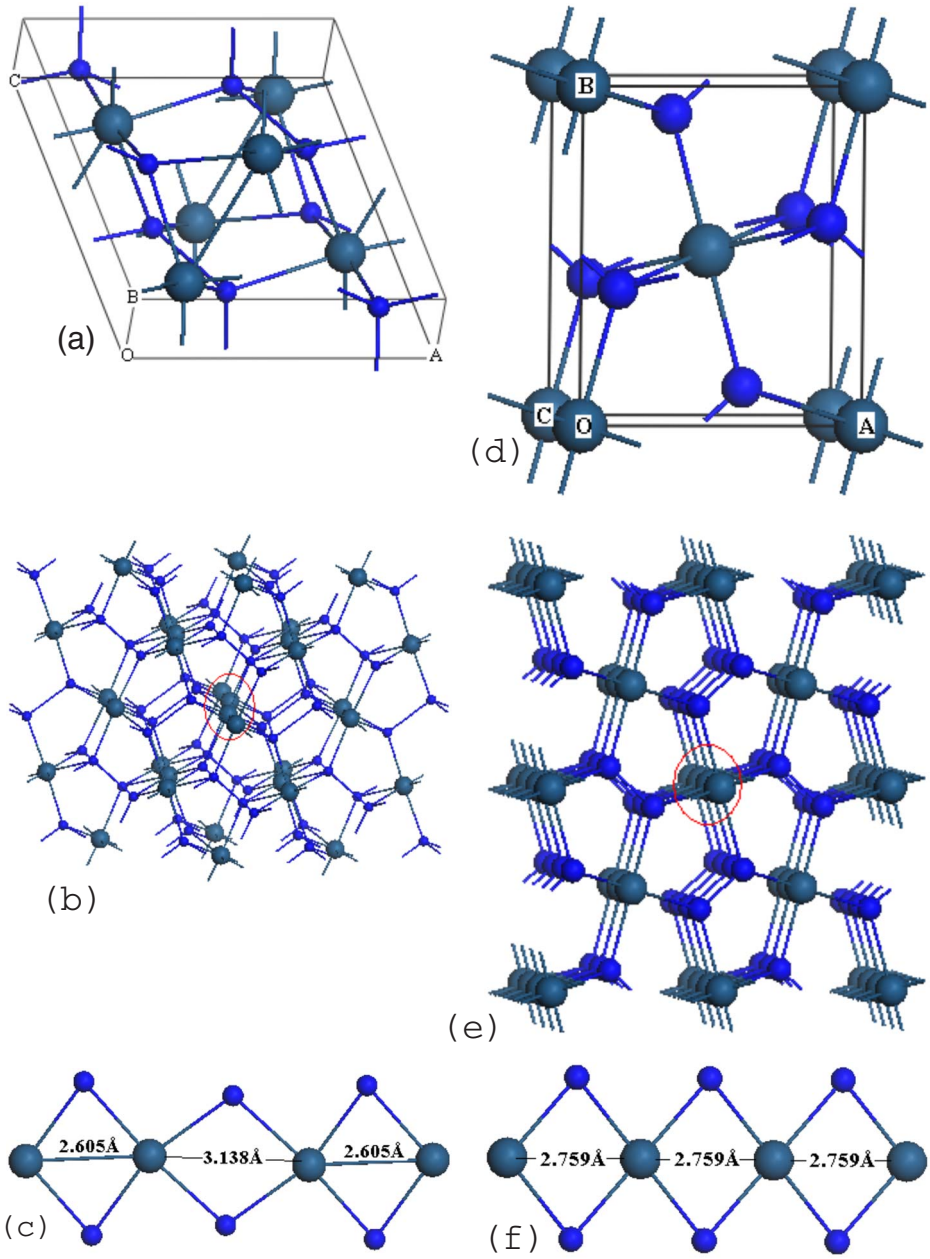

FIG. 1. (Color online) Crystal structure of IrN_2. (a) Monoclinic $P2_1/c$ with arsenopyrite structure, (b) topology of $P2_1/c$ phase in [101] direction, (c) the local environment of the circled Ir atoms in (b), (d) orthorhombic *Pnnm* with marcasite structure, (e) topology of *Pnnm* phase in [001] direction, and (f) the local environment of the circled Ir atoms in (e). The bond distances shown in (c) and (f) are the arithmetic average of LDA and GGA values. The Ir and N atoms are shown in purple (larger) and cyan (smaller) colors, respectively.

and C_{12} are also reasonable compared with the previous theoretical values (although our calculation gave a smaller shear modulus of 65 GPa compared with the previous theoretical value of 92 GPa).[18] For pyrite structure, our calculated value of 337 GPa agrees well with the recent theoretical value of 330 GPa (the average value of LDA and GGA values).[36]

From both the structural data and elastic stiffness constants shown in Tables I and II, it is clear that the most promising phase for IrN_2 is monoclinic $P2_1/c$ [Fig. 1(a)] with arsenopyrite structure. The $P2_1/c$ phase contains 4 f.u. in the conventional cell, in which both Ir and two N atoms occupy Wyckoff 4*e* site. The metal atom Ir is octahedrally coordinated by six N atoms, and N atom is tetrahedrally coordinated by one N and three Ir atoms [Fig. 1(b)]. The IrN_6 octahedra are edge shared in the [101] direction, with the alternating Ir-Ir bond distances of 2.605 and 3.138 Å, respectively [Fig. 1(c)]. Along the [10-1] and *b* directions, the IrN_6 octrahedra are corner shared. For *Pnnm* phase [Fig. 1(d)], the IrN_6 octahedra are edge shared along the *c* axis ([001] direction) and corner shared along *a* and *b* axes [Fig. 1(e)]. The Ir-Ir bond distance along the *c* axis is regular (2.759 Å) [Fig. 1(f)]. For pyrite IrN_2, the IrN_6 octahedra are only corner shared, thus avoiding the close contact between metal atoms (the shortest Ir-Ir bond distance is 3.4 Å). Comparing marcasite *Pnnm* structure with arsenopyrite $P2_1/c$ structure, the alternating short and long Ir-Ir bond distances in $P2_1/c$ lead to a doubling of the translation period in the chain direction ([101] direction). Hence, the arsenopyrite $P2_1/c$ structure can be regarded as a distorted version of the marcasite *Pnnm* structure.

The calculated lattice constants (Table I) are in good agreement compared with the recent theoretical studies.[27,36] The β angle in $P2_1/c$ is 107.8°, smaller than that in IrP_2 (111.58°).[32] It has the lowest energy compared with the other

phases and is mechanically stable (thermodynamically at the LDA level). From Table II, we noticed that our calculated elastic stiffness constants for the $P2_1/c$ phase agree well with the recent theoretical study.[36] The bulk modulus is the largest (373 GPa) (Table II), although it is still smaller than the value of 428 GPa from the experimental study.[16] The calculated shear modulus of 228 GPa is also the largest. Young's modulus and Poisson's ratio are 567 GPa and 0.24, respectively. The small Poisson's ratio for $P2_1/c$ compared with the other phases indicates that the bonding is more directional in the $P2_1/c$ phase. The diatomic N-N has a bond distance of 1.414 Å in the $P2_1/c$ phase, nearly the same as the value of 1.41 Å observed in PtN_2.[15] The value of 1.414 Å is also almost exactly the same as for the single-bonded monatomic nitrogen (triply coordinated) that has been predicted by the previous theoretical study[57] and also reported in a recent experimental study.[58] The low symmetry of the $P2_1/c$ phase is also consistent with the experimental observation that the rich structures of Raman spectrum of IrN_2 suggest either more atoms in the unit cell and/or a less symmetric structure (lower symmetry).[15]

The calculated total density of states (TDOS) shown in Fig. 2 indicates that IrN_2 in the $P2_1/c$ phase is a semiconductor, different from the other phases which are metallic. This agrees with the experimental observation of nonmetallicity in IrN_2.[16] The calculated band gap is indirect with a value of 0.3 eV. Therefore, combined with the fact that IrX_2 (X=P, As, Sb, and Bi), CoP_2, and RhP_2 can be synthesized in monoclinic $P2_1/c$ phase with arsenopyrite-type structure, it is interesting to experimentally examine the crystal structure of IrN_2 in monoclinic $P2_1/c$ phase. On the other hand, the calculated ratio B/G is 1.63, indicating that IrN_2 in the $P2_1/c$ phase is brittle. This is because a high (low) B/G value is associated with ductility (brittleness), and the critical value which separates ductile and brittle materials is about 1.75.[59]

Quite recently, Yu *et al.* reported a theoretical study on OsN_2, IrN_2, RuN_2, and RhN_2 in rutile, fluorite, pyrite, marcasite, and monoclinic arsenopyrite structures.[27] Meanwhile, Wang *et al.* also reported the theoretical study on IrN_2 in fluorite, pyrite, hexagonal, and monoclinic arsenopyrite structures.[36] The investigations showed that for IrN_2, arsenopyrite $P2_1/c$ structure is the most stable phase. The calculated band gap is indirect, with values of 0.3 eV (Ref. 36) and 0.4 eV,[27] in excellent agreement with our calculation (0.3 eV). The insulating behavior was ascribed to be the dimerization of the Ir atoms, which lifts the antibonding states formed by iridium d orbitals.[36] At zero pressure, the energy difference between $Pnnm$ and $P2_1/c$ is 0.16 eV/f.u. in our calculation, nearly the same as 0.15 eV obtained by Yu *et al.*[27] Our calculated diatomic N-N distance is 1.414 Å, in excellent agreement with the recent theoretical value of 1.41 Å.[27] The alternating Ir-Ir bond distances at the LDA level for the $P2_1/c$ phase are 2.58 and 3.09 Å at zero pressure,[27] also in good agreement with our calculated values of 2.599 and 3.129 Å at the LDA level (or 2.605 and 3.138 Å from the arithmetic average of LDA and GGA values). The Ir-Ir atomic pairing for the $P2_1/c$ phase is similar to the pairing mechanism of the quasi-one-dimensional systems upon Peierls distortion.[60] Therefore, as indicated by Yu *et al.*,[27] the distortion from orthorhombic $Pnnm$ to monoclinic $P2_1/c$ phase is the typical Peierls distortion due to the metal-metal interaction in the $P2_1/c$ phase.

Our calculated density of states (DOS) patterns for arsenopyrite $P2_1/c$ and marcasite $Pnnm$ and $Pnn2$ structures (Fig. 2) are consistent with those of Yu *et al.*[27] and Wang *et al.*[36] The lattice constants a=4.861 Å, b=4.907 Å, and c=4.901 Å (Table I) at zero pressure in our calculation match a=4.809 Å, b=4.858 Å, and c=4.848 Å of Yu *et al.*[27] within 1.1% and a=4.8451 Å, b=4.8978 Å, and c=4.8846 Å (the average values of LDA and GGA values) of Wang *et al.*[36] within 0.3%. The β bond angle is within 0.4%. Our calculated bulk modulus of 373 GPa is slightly smaller than 402 GPa from the work of Yu *et al.*,[27] but close to 357 GPa (the average value of LDA and GGA values) from the work of Wang *et al.*[36]

Besides the $P2_1/c$ phase, it is also seen that the two orthorhombic phases $Pnnm$ and $Pnn2$ (i.e., marcasite IrN_2) are also mechanically stable. It is seen from Tables I and II (also Fig. 2) that all the calculated quantities are essentially the same for the two orthorhombic phases. This might be due to the fact that $Pnn2$ is the maximal nonisomorphic subgroup of $Pnnm$. In the case of marcasite IrN_2, the Wyckoff sites are $2a$ for Ir and $4g$ for N in $Pnnm$, and $2a$ for Ir and $4c$ for N in $Pnn2$. The calculated bulk (367 GPa) and shear moduli (222 GPa) for both space groups are also very large. The diatomic N-N distance is shorter (1.376 Å) compared with that (1.414 Å) in the $P2_1/c$ phase.

In order to get further insights into the $Pnnm$ and $P2_1/c$ phases, their partial density of states (PDOS) from Ir $5d$ orbitals and N $2s$, $2p$ orbitals are given in Fig. 3. It is seen that for $Pnnm$, both N $2s$, $2p$ and Ir $5d$ orbitals contribute to the metallic behavior, in particular, N $2p$ and Ir $5d$ orbitals. The DOS of Ir $5d$ is mainly located in the energy region from −5.0 to −1.0 eV. It hybridizes strongly with N $2p$ orbital and, thus, forms covalent bonding. In addition, the calculated net charges on N and Ir are −0.38 and 0.76, respectively. This indicates the existence of ionic bonding between Ir and N. From the charge density distribution [Fig. 4(a)], metallic Ir-Ir bonding in the $Pnnm$ phase is rather weak or can be ignored. Similar to the $Pnnm$ phase, for $P2_1/c$, covalent bonding can be observed from the hybridization of Ir $5d$ with N $2p$ orbitals. The net charge on N1 is −0.37, on N2 is −0.42, and on Ir is 0.79, indicating the ionic bonding in Ir-N bond. In addition, metallic Ir-Ir bonding can be observed for the short Ir-Ir bond distance of 2.605 Å from the charge density distribution [Fig. 4(b)]. Therefore, for $P2_1/c$, there exist mixtures of covalent, ionic, and metallic bondings.

From Table I, we also noticed that for the structures with large diatomic N-N distance (Fm-3m and $P4_2/mnm$ phases), the formation enthalpy is positive and high, indicating the chemical instability. Fluorite structure (Fm-3m) has relatively higher formation enthalpy compared with that of pyrite (Pa-3) (Table I), similar to the case observed in PtN_2 (Ref. 15) and OsN_2.[22]

Next, the relative enthalpies of the different phases compared with both $P2_1/c$ and elements (reactants) as a function of pressure were studied. From Table I, we noticed that at the LDA level, Pa-3 (−0.45 eV), $Pnnm$ (−0.78 eV), $Pnn2$

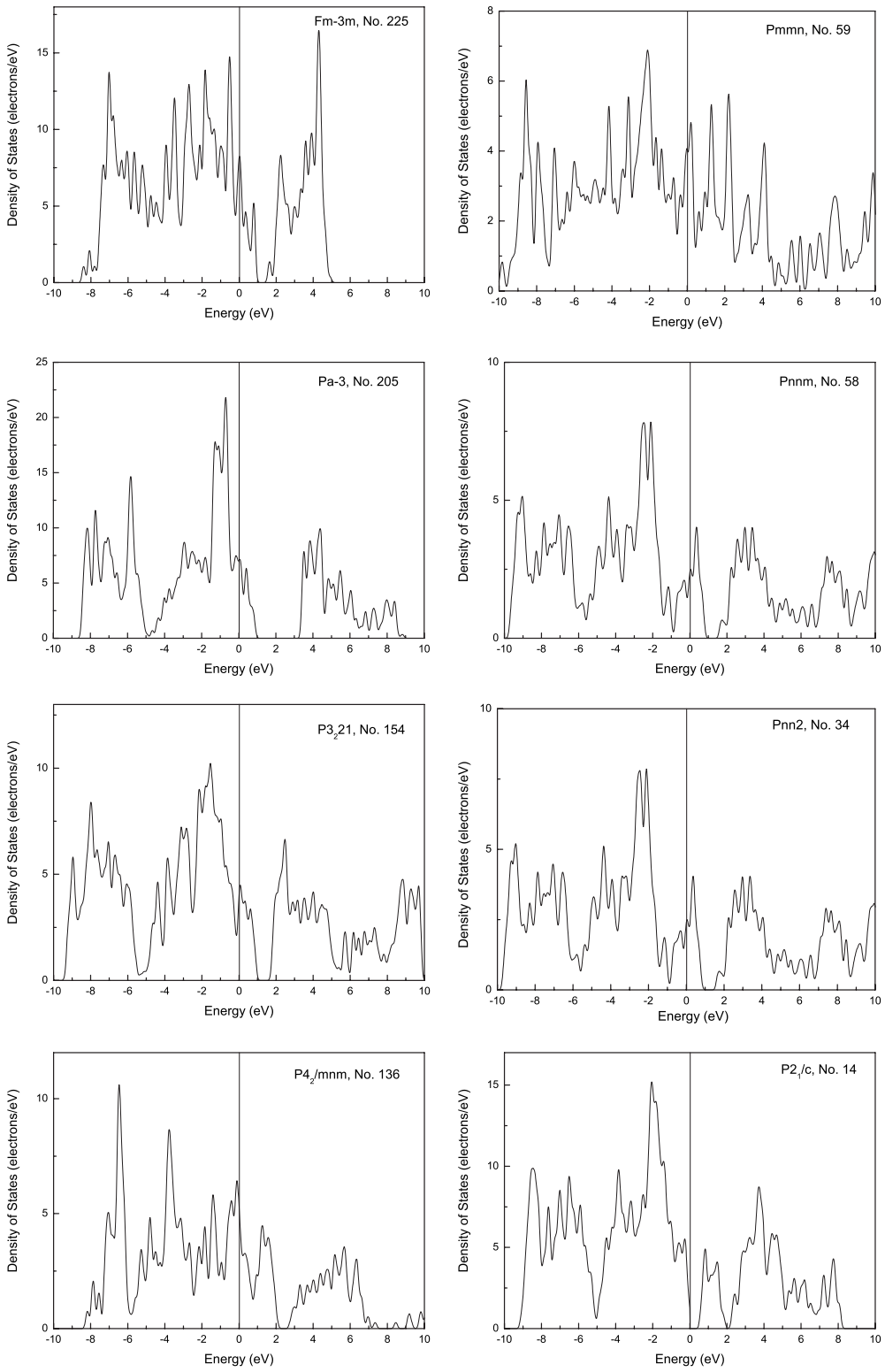

FIG. 2. Total density of states (TDOS) for each assumed space group in IrN_2. The Fermi energy level is at zero.

(−0.78 eV), and $P2_1/c$ (−0.94 eV) are thermodynamically stable at zero pressure because of their negative formation enthalpy. While at GGA level, all the phases are thermodynamically unstable. In the following, for brevity, we only calculate the formation enthalpy of the three phases i.e., pyrite *Pa*-3, marcasite *Pnnm*, and arsenopyrite $P2_1/c$, at the GGA level as a function of pressure. It is seen from Fig. 5(a) that, at the GGA level, the three phases become stable compared with its constituents at above approximately 3 GPa for $P2_1/c$, 6 GPa for *Pnnm*, and 9 GPa for *Pa*-3. This is consistent with the experimental finding that the compound was synthesized at the pressure of 50 GPa.[15,16] On this aspect, it

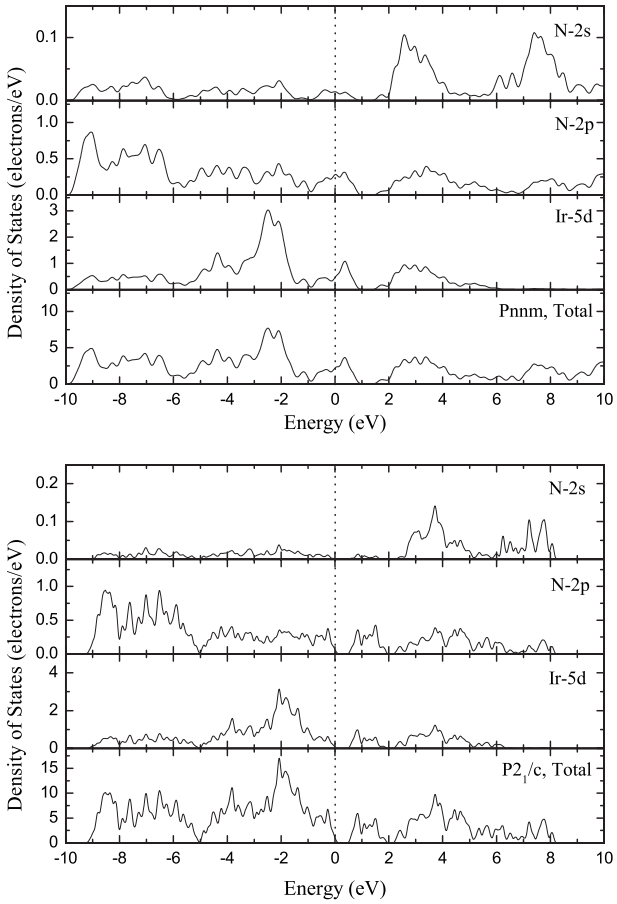

FIG. 3. Total and partial densities of states (DOS) for IrN_2 for space groups *Pnnm* (top) and $P2_1/c$ (bottom). The Fermi energy level is at zero.

is interesting to note that PtN_2 was synthesized at 45–50 GPa.[9,15] Theoretical studies on PtN_2 indicated that pyrite PtN_2 becomes thermodynamically stable above approximately 11 GPa (Ref. 14) and 16.7 GPa.[25] For OsN_2, marcasite structure becomes stable above 23 GPa,[25] consistent with the experimental finding that it can be synthesized when the pressure reaches 50 GPa.[16]

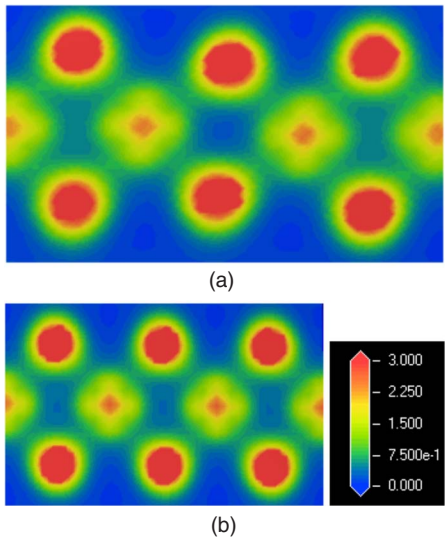

FIG. 4. (Color online) Charge density distributions of IrN_2 in (a) *Pnnm* in Fig. 1(c) and (b) $P2_1/c$ in Fig. 1(f).

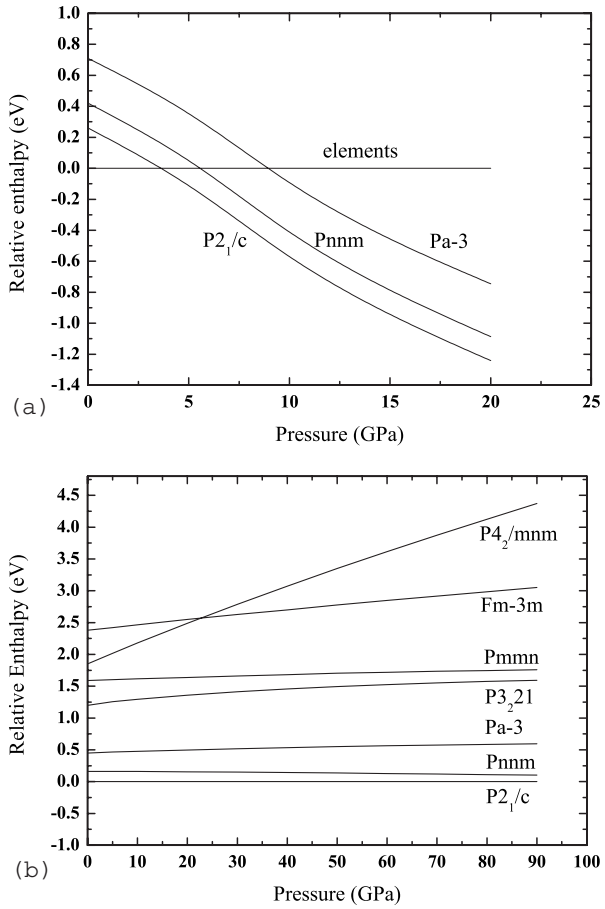

FIG. 5. (a) Plots of relative enthalpies (per f.u.) of elements Ir $+N_2$ compared with IrN_2 at $P2_1/c$, *Pnnm*, and *Pa*-3 phases as a function of pressure. (b) Plots of relative enthalpies (per f.u.) between $P2_1/c$ and the other space groups as a function of pressure at the GGA level.

From Fig. 5(b), it is seen that $P2_1/c$ is the most stable phase for IrN_2 at above 100 GPa. In fact, a displacive phase transition from distorted semiconducting $P2_1/c$ to undistorted metallic *Pnnm* phase occurs at much higher pressure, i.e., near 300 GPa at GGA level and 200 GPa at the LDA level. Our calculated transition pressure is much higher than 200 GPa at the GGA level[61] and 165 GPa at the LDA level[27] as obtained by Yu *et al.* This might be due to the fact that the transition pressure determined from the enthalpy-pressure relationship is suitable only for the first-order transitions. While considering the symmetry and atomic coordination, however, the transition of IrN2 from arsenopyrite $P2_1/c$ to marcasite *Pnnm* structure is of the second order. That is to say, the enthalpy of the arsenopyrite $P2_1/c$ structure should merge with that of the marcasite *Pnnm* structure asymptotically, and the transition pressure is ill-defined in the enthalpy-pressure curves.[27,61]

TABLE III. Formation enthalpy per formula unit ΔE (eV), lattice constant a (Å), density ρ (g/cm^{-3}), cell volume per formula unit V (Å^3), fractional coordinates of N, and the shortest N1-N1 and Ir-N and second shortest N2-N2 bond distances (Å) at the GGA and LDA levels for IrN_3. "Ave." is the average of GGA and LDA values.

		ΔE	a	ρ	V	Fractional coordinates of N $(0,y,z)$	N1-N1	N2-N2	Ir-N
IrN_3-I	GGA	0.50	6.871	9.604	40.5	0.0, 0.3072, 0.0925	1.271	2.650	2.068
	LDA	−0.92	6.802	9.897	39.3	0.0, 0.3086, 0.0937	1.274	2.603	2.045
	Ave.		6.836	9.750	39.9		1.272	2.626	2.056
IrN_3-II	GGA	1.87	6.602	10.804	36.0	0.0, 0.3804, 0.1119	1.478	1.579	2.073
	LDA	0.12	6.552	11.081	35.1	0.0, 0.3799, 0.1126	1.476	1.574	2.054
	Ave.		6.577	10.942	35.5		1.477	1.576	2.063

IrN_3

The calculated lattice constants and elastic stiffness constants were listed in Tables III and IV, respectively. The conventional cell of IrN_3 contains 8 f.u. Iridium occupies the Wyckoff 8*c* site $(1/4,1/4,1/4)$, and nitrogen at 24*g* site $(0,y,z)$. In our calculation, by choosing different initial geometries, two local minima or modifications were found on the potential energy surface (Fig. 6). The first one, termed as IrN_3-I or I [Fig. 6(c)], is lower in energy (1.36 eV at the GGA level and 1.04 eV at the LDA level, per formula unit, Table III) than the second one, IrN_3-II or II [Fig. 6(f)].

From the structural point of view, it is interesting to note that for both modifications, Ir atoms form a simple cubic framework with the Ir-Ir bond distance of 3.435 Å in modification I [Fig. 6(a)] and 3.301 Å in modification II [Fig. 6(d)]. Ir atom is coordinated by six nitrogen atoms, forming an octahedron [Fig. 7(a)]. The octahedra are connected by corners [Fig. 7(b)]. In addition, we noticed that in modification I, the diatomic N-N unit N_2 has a very short bond distance of 1.271 Å. The two N_2 are well separated by a large distance (2.649 Å) [Fig. 6(b)] and form a rectangular shape. This results in the coordination number of N being 3, i.e., one nitrogen atom and two Ir atoms. The system is metallic (for details, see below). For modification II, N-N forms diatomic N-N unit N_2 with a long distance of 1.478 Å, and the two N_2 are connected by a relatively short distance of 1.579 Å (compared with 2.649 Å in modification I) and form a quasisquare shape [Fig. 6(e)]. The coordination number of N is 4, i.e., two nitrogen atoms and two Ir atoms [Fig. 7(c)]. The resulting system is nonmetallic (for details, see below) and has a relatively higher energy. The calculated cell volume per formula unit shows that modification II (35.5 Å^3) is more compact or denser than modification I (39.9 Å^3) (Table III). The relatively lower energy in modification I is mainly due to the short N-N bond distance of 1.271 Å. This is demonstrated by our calculation on the isolated 4N system, as shown in Fig. 8. It is seen that the 4N system in IrN_3-I is lower in energy by 6.64 eV than that in IrN_3-II, or 3.32 eV for each diatomic N-N unit N_2.[62] The change of energy as a function of N fractional coordinates was given in Fig. 9, in which an energy barrier can be seen clearly in going from modification I to II.

The above mentioned two modifications were also found in PtN_3 and RhN_3 with skutterudite-type structure from our calculation. It turns out that the two modifications of PtN_3 are mechanically unstable, while those of RhN_3 are mechanically stable. At the GGA level, the calculated bulk modulus of RhN_3 is 244 GPa for modification II (with higher energy) and 166 GPa for modification I (with lower energy). We did not proceed with further calculation on RhN_3 because the phenomena observed in RhN_3 are similar to those in IrN_3. IrN_3 could serve as a good example and is more interesting because it has much higher bulk modulus than RhN_3. For IrP_3, however, the above mentioned two modifications were not found. Only modification II was obtained when choosing different initial geometries. This might be due to the fact that P (atomic radius of 1.105 Å) is larger than N (atomic radius of 0.92 Å). Thus, in IrP_3, the bond distance of diatomic P-P unit P_2 becomes large (2.220 Å) after geometry optimiza-

TABLE IV. Elastic stiffness constants C_{ij}, bulk modulus B (GPa), shear modulus G (GPa), Young's modulus E (GPa), Poisson's ratio ν, anisotropic factor A, and Debye temperature θ_D (K) at the GGA and LDA levels for IrN_3. "Ave." is the average of GGA and LDA values.

		C_{11}	C_{44}	C_{12}	B	G	E	ν	A	θ_D
IrN_3-I	GGA	479	140	124	242	154	381	0.24	0.84	611
	LDA	543	151	155	284	167	419	0.25	0.84	634
	Ave.	511	145	139	263	160	400	0.24	0.84	622
IrN_3-II	GGA	607	273	206	339	241	585	0.21	1.24	748
	LDA	648	290	241	377	251	617	0.23	1.27	762
	Ave.	627	281	223	358	246	601	0.22	1.25	755

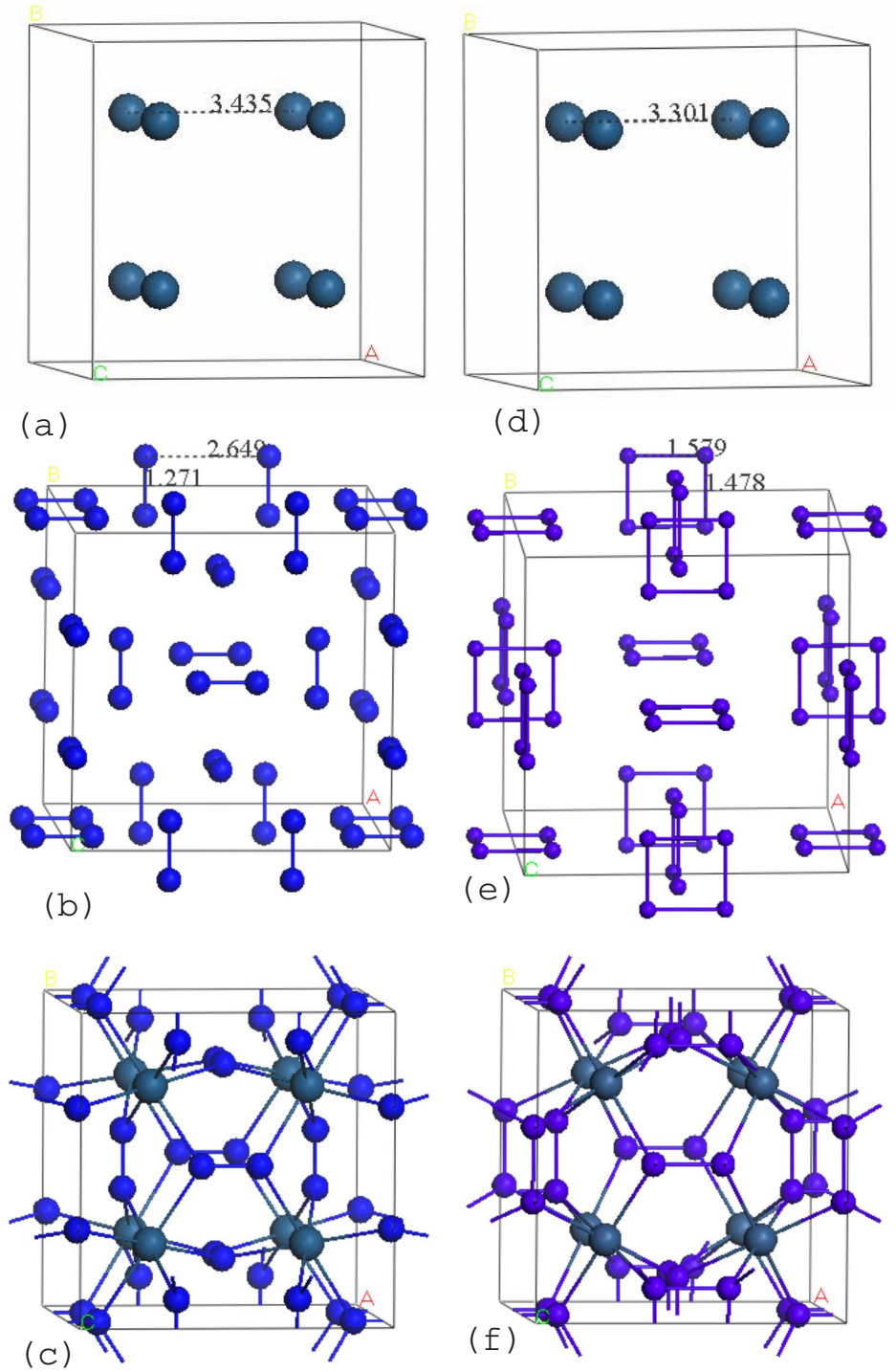

FIG. 6. (Color online) Optimized crystal structures of cubic IrN_3-I (c) and IrN_3-II (f). The crystal structure (c) [(f)] is obtained by the combination of two separate parts, Ir framework (a) [(d)] and nitrogen framework (b) [(e)], i.e., $a+b=c$. The bond distances shown in (a), (b), (d), and (e) are from GGA calculation (see also Table III). The Ir and N atoms are shown in purple (larger) and cyan (smaller), respectively.

tion, and both modifications converged to one structure (modification II). The two P_2 join together with a distance of 2.325 Å and forms a quasisquare shape. The coordination number of P is 4, i.e., two P atoms and two Ir atoms.

From the calculated elastic stiffness constants shown in Table IV, it is seen that for IrN_3, the two modifications are mechanically stable. Modification II has a larger bulk modulus of 358 GPa compared with 263 GPa in modification I, indicating that modification II is less compressible than I. This is consistent with the smaller volume of modification II than that of I (Table III). In addition, the calculated shear modulus of 246 GPa and Young's modulus of 601 GPa in modification II are also larger than the corresponding values of 160 and 400 GPa in modification I. The calculated anisotropic factors $A=(2C_{44}+C_{12})/C_{11}$ are 0.84 and 1.24 for modifications I and II, respectively. This reveals that both modifications are anisotropic, because a value of 1 represents completely elastic isotropy, while values smaller or greater than 1 measure the degree of elastic anisotropy.

Compared with arsenopyrite IrN_2, IrN_3 has a slightly smaller bulk modulus (358 GPa for modification II compared with 373 GPa in IrN_2). Nonetheless, for IrN_3, the cal-

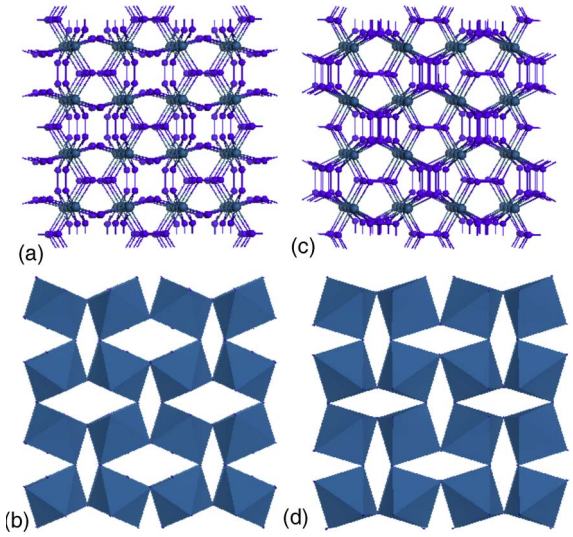

FIG. 7. (Color online) (a) Topology of IrN_3-I, (b) connection of octahedra in IrN_3-I, (c) topology of IrN_3-II, and (d) connection of octahedra in IrN_3-II. The Ir and N atoms are shown in purple (larger) and cyan (smaller), respectively.

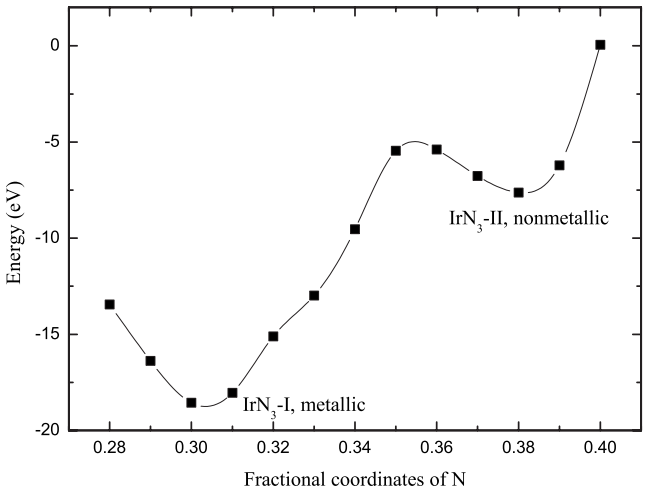

FIG. 9. Energy vs fractional coordinate of N (y) in IrN_3. The absolute energy is obtained by adding −11 000 eV. For the z component of N fractional coordinates (0.0, y, z), since it changes slightly from modification I (0.09) to II (0.11), we chose three points for each y value, i.e., 0.09, 0.10, and 0.11. Among the three points, the structure with the lowest energy after optimization was selected and shown in the figure. During the geometry optimization, only the fractional coordinates of N were fixed; other parameters such as lattice constants were allowed to relax.

culated shear modulus, a better indicator for hardness compared with bulk modulus, is 246 GPa, slightly larger than 228 GPa in IrN_2. Young's modulus is 601 GPa in IrN_3, larger than 568 GPa in IrN_2, while Poisson's ratio is 0.22 in IrN_3, smaller than 0.24 in IrN_2. The small Poisson's ratio indicates that the bonding is more directional. Thus, the above results are clear indication that IrN_3 could be a potential candidate to be superhard.

The calculated TDOS shows that modification I is metallic because of the finite $N(E_F)$ at the Fermi level (Fig. 10, top). However, due to the small $N(E_F)$ at the Fermi energy level, modification I is a poor conductor. The conducting behavior is mainly caused by N $2p$ orbital as seen from the partial DOS of Fig. 10 (top). Ir $5d$ orbital shows much weaker conductivity and can actually be ignored (see the inset of IrN_3-I in Fig. 10, top). This is different from modification II, in which both N and Ir are nonmetallic (see the DOS of IrN_3-II in Fig. 10, bottom). The calculated band gap for modification II is 0.65 eV. The bonding between two diatomic N-N unit N_2 can be clearly seen from charge density distributions shown in Fig. 11. From the PDOS of both modifications, we also noticed that Ir $5d$ orbital has a strong hybridization with N $2p$ orbital, indicating the covalent bonding. In addition, both TDOS and PDOS patterns are different between the two modifications.

Atomic population gave the net charges of 0.85 on Ir and −0.28 on N in modification I, indicating the existence of ionic bonding, whereas for modification II, the net charges on Ir and N are 0.77 and −0.26, respectively. The smaller charge transfer in modification II suggests that it is less ionic compared with modification I.

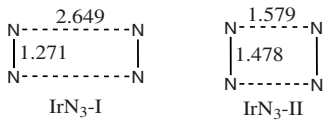

FIG. 8. In the two isolated 4N systems, IrN_3-I is 6.64 eV lower in energy than IrN_3-II, or 3.32 eV per diatomic N-N unit N_2.

From Fig. 11, it is seen that metallic Ir-Ir bonding does not exist in both modifications. For modification I, it seems that metallic bonding were observed in (110) plane. In fact, the small charge density between Ir atoms in (110) plane is from the projection of N_2 above the plane. This is confirmed by the charge density plot in (100) plane (Fig. 11, right). In (100) plane, Ir atoms form a square planar structure, i.e., the bond distances Ir1-Ir2, Ir1-Ir3, Ir2-Ir4, and Ir3-Ir4 are equal. From Fig. 11 (right), it is seen that metallic bonding does not exist between Ir1-Ir3 and Ir2-Ir4, which should also be true for Ir1-Ir2 and Ir3-Ir4 bonds. Therefore, the charge density between Ir1-Ir2 and Ir3-Ir4 should be from other atoms. Our careful checking indicates that it is from the projection of N_2 above the Ir-Ir bond. In addition, the charge density between Ir atoms is not located in the middle of the axis of the Ir-Ir bond, which should be another indication that the charge density is not contributed by the two Ir atoms. The reason that the charge density between Ir atoms is seen in modification I (Fig. 11, left), not in II (Figure 11, middle), is because in modification I, the distance between Ir square plane and diatomic N-N unit N_2 above it is much closer in I [Fig. 6(c)] than in II [Fig. 6(f)]. In other words, metallic bonding does not exist for the long Ir-Ir bond distance in both modifications [3.435 Å in I/and 3.301 Å in II at the GGA level, see Figs. 6(a) and 6(d)]. Thus, for both modifications, there exists a mixture of covalent and ionic bondings. This is different from IrN_2 in the most stable $P2_1/c$ phase, in which, besides covalent and ionic bondings, metallic bonding is also obvious [Ir-Ir bond with the distance of 2.605 Å in IrN_2, Fig. 1(c)]. Therefore, our calculation suggests that the intercala-

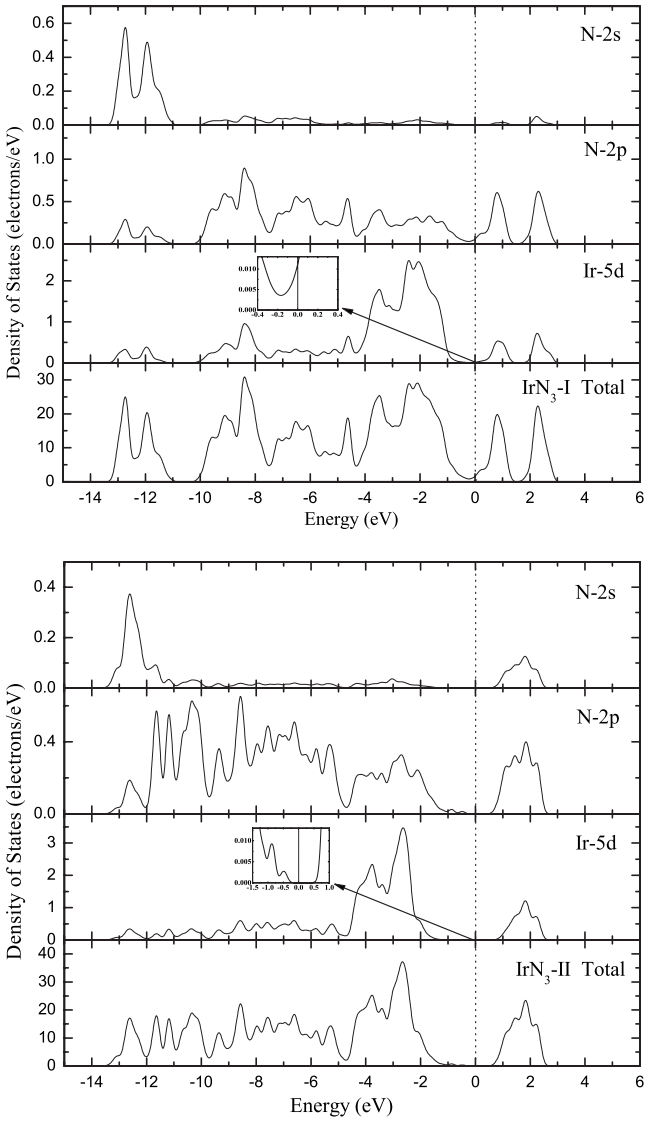

FIG. 10. Calculated total and partial DOS of IrN_3-I (top) and IrN_3-II (bottom). Vertical dotted line indicates the Fermi energy. The insets in both pictures (top and bottom) are the partial DOS of Ir 5*d* orbital near the Fermi energy level.

tion of the dinitrogen units into the Ir lattice induces a substantial change of the electronic structure from metallic, in bulk Ir, to a mixture of covalent and ionic bondings in IrN_3.

The calculated ratio B/G for modification I is 1.64 and for modification II is 1.45, indicating that they are brittle, in particular, for modification II.

In the following, we have calculated the Debye temperature.[63] It is known that as a fundamental parameter, Debye temperature correlates with many physical properties of solids, such as specific heat, elastic stiffness constants, and melting temperature. At low temperatures, the vibrational excitations arise solely from acoustic vibrations. Therefore, the Debye temperature calculated from elastic stiffness constants at low temperatures is the same as that determined from specific heat measurements. The calculated Debye temperature is 622 K for modification I, smaller than 755 K for modification II. Since at low temperatures only the acoustic

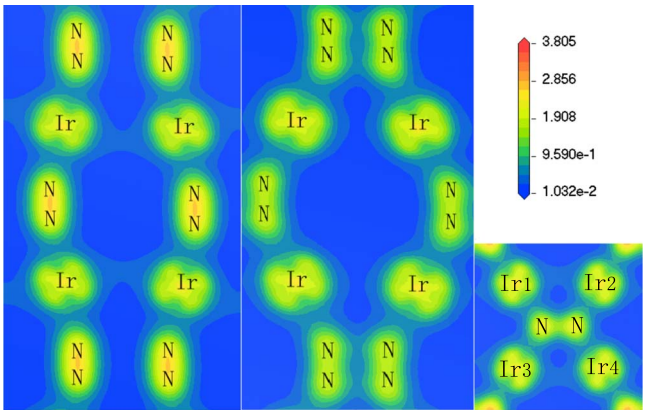

FIG. 11. (Color online) Charge density distributions of IrN_3-I (left), IrN_3-II (middle) in (110) plane, and IrN_3-I in (100) plane (right).

branches of phonons are active, therefore, the estimated Debye temperature from our elastic stiffness constants is valid for low temperatures.

Finally, both modifications were studied as a function of pressure. Similar to IrN_2, we only calculated the formation enthalpy of both modifications at the GGA level. It is seen from Fig. 12(a) that modifications I and II become thermodynamically stable compared with elements at above approximately 2 and 11 GPa, respectively. This is, indeed, an interesting conclusion since experimental studies on iridium nitride were conducted at above 50 GPa, but only iridium nitride with stoichiometry of 1:2 (i.e., IrN_2) was confirmed.[15,16] Therefore, we suggest that IrN_3 should be examined in further experimental studies. On the other hand, modification II becomes energetically favorable than I above 64 GPa [Fig. 12(b)].

CONCLUSIONS

IrN_2 was studied for various crystal structures. We predict that IrN_2 in monoclinic $P2_1/c$ phase of arsenopyrite structure with even formula units is semiconducting and very promising to be superhard. This is in good agreement with both the experimental and recent theoretical studies.

From our calculation, arsenopyrite IrN_2 contains mixtures of covalent, ionic, and metallic bondings. The bond distance of diatomic N-N unit N_2 is 1.414 Å. Compared with the other phases, IrN_2 remains stable at very high pressure. A displacive phase transition from distorted semiconducting $P2_1/c$ to undistorted metallic *Pnnm* phase occurs at around 300 GPa at the GGA level and 200 GPa at the LDA level. The $P2_1/c$ phase becomes energetically favorable above 3 GPa compared with the reactants $Ir+N_2$ at GGA level. The calculated bulk modulus is 373 GPa and shear modulus is 228 GPa. The obtained value of 373 GPa matches the recent theoretical values of 357 GPa within 4.3% and of 402 GPa within 7.8%, but smaller than the experimental value of 428 GPa by 14.7%.

For IrN_2, marcasite *Pnnm* and *Pnn*2 phases are also very promising to be superhard. The bond distance of diatomic

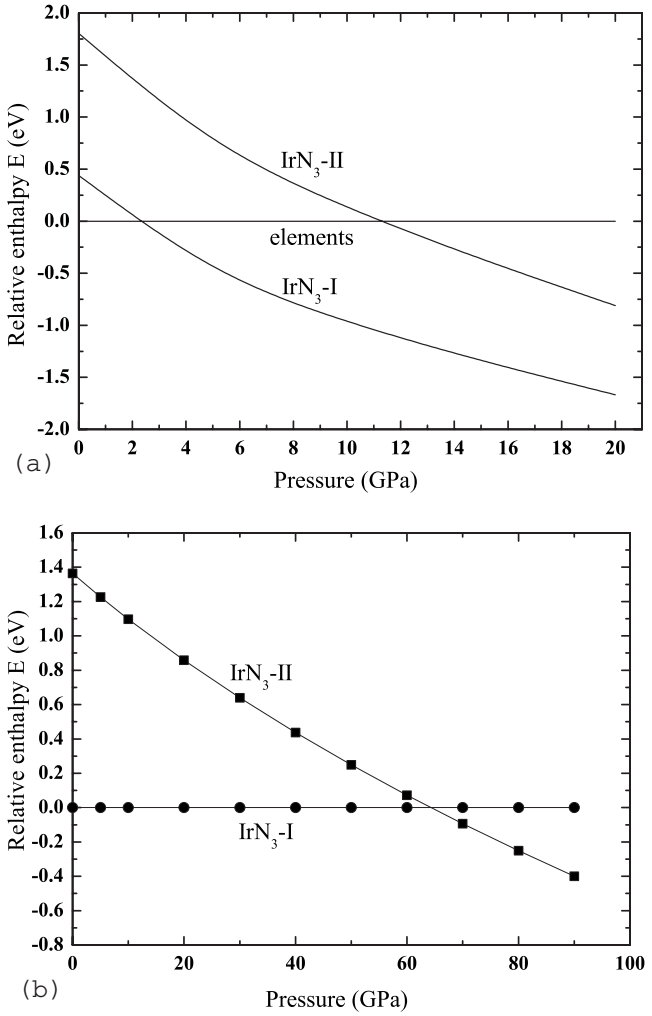

FIG. 12. (a) Plots of relative enthalpies (per f.u.) between elements $Ir+(3/2)N_2$ and IrN_3-I, IrN_3-II as a function of pressure. (b) Plots of relative enthalpies (per f.u.) between IrN_3-I and IrN_3-II as a function of pressure at the GGA level.

N-N unit N_2 is 1.376 Å. The calculated bulk modulus is 367 GPa and shear modulus is 222 GPa. It becomes energetically favorable above 6 GPa compared with the reactants $Ir+N_2$ at the GGA level. The metallic behavior in both phases is mainly from Ir $5d$ and N $2p$ orbitals.

In addition, we also predict that IrN_3 with cubic skutterudite structure is very promising to be superhard. Two local minima or modifications (termed as I and II) were located for IrN_3. Modification I is a poor metal, while II is nonmetallic. Modification I is energetically more stable than II by around 1.2 eV/f.u. (the arithmetic average of GGA and LDA values, Table III). Thermodynamically stable phases were observed at above approximately 2 and 11 GPa for modifications I and II, respectively. The two modifications are different due to the different arrangement of N atoms. Short N-N bond distance of 1.272 Å is observed in modification I. Because of the smaller size of nitrogen, modification I is unique since the corresponding structure cannot be observed in IrP_3.

The calculated bulk modulus is 263 GPa for modification I and is 358 GPa for modification II. Modification II becomes energetically favorable than I above 64 GPa. Both modifications are brittle. The calculated elastic anisotropic factors for both modifications indicate that they are elastically anisotropic. We wish our study could stimulate future experimental study.

ACKNOWLEDGMENTS

Z.J.W. is grateful to Rong Yu for comments on the paper, in particular, on the transition pressure from a marcasite structure to an arsenopyrite one, and Richard Dronskowski for stimulating discussions. We are also grateful to Zhong Feng for proofreading the paper. The authors thank the National Natural Science Foundation of China (NNSFC) for financial support (Grants No. 20331030 and No. 20571073).

*Corresponding author. zjwu@ciac.jl.cn

[1] J. Hanies, J. M. Léger, and G. Bocquillon, Annu. Rev. Mater. Res. **31**, 1 (2001).
[2] R. B. Kaner, J. J. Gilman, and S. H. Tolbert, Science **308**, 1268 (2005).
[3] F. J. Ribeiro, P. Tangney, S. G. Louie, and M. L. Cohen, Phys. Rev. B **74**, 172101 (2006).
[4] Z. Y. Liu, J. L. He, J. Yang, X. J. Guo, H. Sun, H. T. Wang, E. D. Wu, and Y. J. Tian, Phys. Rev. B **73**, 172101 (2006).
[5] J. L. He, L. C. Guo, X. J. Guo, R. P. Liu, Y. J. Tian, H. T. Wang, and C. X. Gao, Appl. Phys. Lett. **88**, 101906 (2006).
[6] E. Horvath-Bordon, R. Riedel, A. Zerr, P. F. McMillan, G. Auffermann, Y. Prots, W. Bronger, R. Kniep, and P. Kroll, Chem. Soc. Rev. **35**, 987 (2006).
[7] A. Zerr, G. Miehe, and R. Riedel, Nat. Mater. **2**, 185 (2003).
[8] E. Gregoryanz, C. Sanloup, M. Somayazulu, J. Brado, G. Fiquet, H.-K. Mao, and R. J. Hemley, Nat. Mater. **3**, 294 (2004).
[9] M. Mattesini, R. Ahuja, and B. Johansson, Phys. Rev. B **68**, 184108 (2003).
[10] P. Kroll, Phys. Rev. Lett. **90**, 125501 (2003).
[11] M. Xu, S. Y. Wang, G. Yin, J. Li, Y. X. Zheng, L. Y. Chen, and Y. Jia, Appl. Phys. Lett. **89**, 151908 (2006).
[12] P. Kroll, T. Schröter, and M. Peters, Angew. Chem., Int. Ed. **44**, 4249 (2005).
[13] S. K. R. Patil, S. V. Khare, B. R. Tuttle, J. K. Bording, and S. Kodambaka, Phys. Rev. B **73**, 104118 (2006).
[14] J. von Appen, M.-W. Lumey, and R. Dronskowski, Angew. Chem., Int. Ed. **45**, 4365 (2006).
[15] J. C. Crowhurst, A. F. Goncharov, B. Sadigh, C. L. Evans, P. G. Morrall, J. L. Ferreira, and A. J. Nelson, Science **311**, 1275 (2006).
[16] A. F. Young, C. Sanloup, E. Gregoryanz, S. Scandolo, R. J. Hem-

ley, and H. K. Mao, Phys. Rev. Lett. **96**, 155501 (2006).
[17] R. Yu and X. F. Zhang, Appl. Phys. Lett. **86**, 121913 (2005).
[18] R. Yu and X. F. Zhang, Phys. Rev. B **72**, 054103 (2005).
[19] R. Yu, Q. Zhan, and X. F. Zhang, Appl. Phys. Lett. **88**, 051913 (2006).
[20] H. Y. Gou, L. Hou, J. W. Zhang, G. F. Sun, L. H. Gao, and F. M. Gao, Appl. Phys. Lett. **89**, 141910 (2006).
[21] A. F. Young, J. A. Montoya, C. Sanloup, M. Lazzeri, E. Gregoryanz, and S. Scandolo, Phys. Rev. B **73**, 153102 (2006).
[22] C. Z. Fan, S. Y. Zeng, L. X. Li, Z. J. Zhan, R. P. Liu, W. K. Wang, P. Zhang, and Y. G. Yao, Phys. Rev. B **74**, 125118 (2006).
[23] Z. J. Wu, X. F. Hao, X. J. Liu, and J. Meng, Phys. Rev. B **75**, 054115 (2007).
[24] Z. W. Chen *et al.*, Phys. Rev. B **75**, 054103 (2007).
[25] J. A. Montoya, A. D. Hernandez, C. Sanloup, E. Gregoryanz, and S. Scandolo, Appl. Phys. Lett. **90**, 011909 (2007).
[26] Y. X. Wang, M. Arai, and T. Sasaki, Appl. Phys. Lett. **90**, 061922 (2007).
[27] R. Yu, Q. Zhan, and L. C. De Jonghe, Angew. Chem., Int. Ed. **46**, 1136 (2007).
[28] D. B. Rogers, R. D. Shannon, A. W. Sleight, and J. L. Gillson, Inorg. Chem. **8**, 841 (1969).
[29] B. Aronsson, Acta Chem. Scand. (1947-1973) **17**, 3026 (1963).
[30] M. J. Buerger, Zeit. Kristallographie, Kristallgeometrie, Kristallphysik, Kristallchemie **97A**, 504 (1937).
[31] G. Brostigen and A. Kjekshus, Acta Chem. Scand. (1947-1973) **24**, 1925 (1970).
[32] A. Kjekshus, Acta Chem. Scand. (1947-1973) **25**, 411 (1971).
[33] G. S. Zhdanov and R. N. Kuz'min, Kristallografiya **6**, 704 (1961) [Sov. Phys. Crystallogr. **6**, 704 (1961)].
[34] N. N. Zhuravlev and E. M. Smirnova, Kristallografiya **10**, 694 (1965) [Sov. Phys. Crystallogr. **10**, 694 (1965)].
[35] W. Jeitschko, U. Flörke, and U. D. Scholz, J. Solid State Chem. **52**, 320 (1984).
[36] Y. X. Wang, M. Arai, T. Sasaki, and C. Z. Fan, Phys. Rev. B **75**, 104110 (2007).
[37] T. Lundström, Ark. Kemi **30**, 115 (1969).
[38] H. P. Woods, F. E. Wawner, Jr., and B. G. Fox, Science **151**, 75 (1966).
[39] S. La Placa and B. Post, Acta Crystallogr. **15**, 97 (1962).
[40] V. I. Khitrova, Kristallografiya **6**, 439 (1962) [Sov. Phys. Crystallogr. **6**, 439 (1962)].
[41] S. Rundqvist and N.-O. Ersson, Ark. Kemi **30**, 103 (1968).
[42] A. Kjekshus and G. Pedersen, Acta Crystallogr. **14**, 1065 (1961).
[43] S. Scandolo (private communication).
[44] M. D. Segall, P. J. D. Lindan, M. J. Probert, C. J. Pickard, P. J. Hasnip, S. J. Clark, and M. C. Payne, J. Phys.: Condens. Matter **14**, 2717 (2002).
[45] D. Vanderbilt, Phys. Rev. B **41**, 7892 (1990).
[46] H. J. Monkhorst and J. D. Pack, Phys. Rev. B **13**, 5188 (1976); J. D. Pack and H. J. Monkhorst, *ibid.* **16**, 1748 (1977).
[47] D. M. Ceperley and B. J. Alder, Phys. Rev. Lett. **45**, 566 (1980); J. P. Perdew and A. Zunger, Phys. Rev. B **23**, 5048 (1981).
[48] J. P. Perdew, K. Burke, and M. Ernzerhof, Phys. Rev. Lett. **77**, 3865 (1996).
[49] J. A. Venables and C. A. English, Acta Crystallogr., Sect. B: Struct. Crystallogr. Cryst. Chem. **30**, 929 (1974).
[50] W. Voigt, *Lehrburch der Kristallphysik* (Teubner, Leipzig, 1928).
[51] A. Reuss, Z. Angew. Math. Mech. **9**, 49 (1929).
[52] R. Hill, Proc. Phys. Soc. London **65**, 350 (1952).
[53] J. P. Watt and L. Peselnick, J. Appl. Phys. **51**, 1525 (1980).
[54] J. P. Watt, J. Appl. Phys. **50**, 6290 (1980).
[55] J. P. Watt, J. Appl. Phys. **51**, 1520 (1980).
[56] J. F. Nye, *Physical Properties of Crystals* (Oxford University Press, Oxford, 1985).
[57] C. Mailhiot, L. H. Yang, and A. K. McMahan, Phys. Rev. B **46**, 14419 (1992).
[58] M. I. Eremets, A. G. Gavriliuk, I. A. Trojan, D. A. Dzivenko, and R. Boehler, Nat. Mater. **3**, 558 (2004).
[59] S. F. Pugh, Philos. Mag. **45**, 823 (1954).
[60] R. E. Peierls, *Quantum Theory of Solids* (Oxford University Press, London, 1955).
[61] R. Yu (private communication).
[62] Single point energy calculation was done using GAUSSIAN 03. The method used is B3LYP [A. D. Becke, J. Chem. Phys. **98**, 5648 (1993); C. Lee, W. Yang and R. G. Parr, Phys. Rev. B **37**, 785 (1988)]. The basis set used is 6-311++G(*df*). For GAUSSIAN 03, please see M. J. Frisch *et al.*, GAUSSIAN 03, Gaussian, Inc., Pittsburgh, PA, 2003.
[63] O. L. Anderson, J. Phys. Chem. Solids **24**, 909 (1963).